Journal of large-scale research facilities

Journal of large-scale research facilities, 4, A133 (2018) http://dx.doi.org/10.17815/jlsrf-4-168

Published: 31.10.2018

The High Enthalpy Shock Tunnel Göttingen of the German Aerospace Center (DLR)

Deutsches Zentrum für Luft - und Raumfahrt (DLR)

Institute of Aerodynamics and Flow Technology *

Instrument Scientists:

- Prof. Dr. Klaus Hannemann, DLR, Institute of Aerodynamics and Flow Technology, phone: +49 (0) 551 709-2477, email: klaus.hannemann@dlr.de
- Dr. Jan Martinez Schramm, DLR, Institute of Aerodynamics and Flow Technology, phone: +49 (0) 551 709-2323, email: jan.martinez@dlr.de
- Dr. Alexander Wagner, DLR, Institute of Aerodynamics and Flow Technology, phone: +49 (0) 551 709-2648, email: alexander.wagner@dlr.de
- Giannino Ponchio Camillo, DLR, Institute of Aerodynamics and Flow Technology, phone: +49 (0) 551 709-2749, email: giannino.ponchiocamillo@dlr.de

Abstract: The High Enthalpy Shock Tunnel Göttingen (HEG) of the German Aerospace Center (DLR) is one of the major European hypersonic test facilities. It was commissioned for use in 1991 and was utilized since then extensively in a large number of national and international space and hypersonic flight projects. Originally, the facility was designed for the investigation of the influence of high temperature effects such as chemical and thermal relaxation on the aerothermodynamics of entry or re-entry space vehicles. Over the last years its range of operating conditions was subsequently extended. In this framework the main emphasis was to generate test conditions which allow investigating the flow past hypersonic flight configuration from low altitude Mach 6 up to Mach 10 in approximately 33 km altitude. The studies performed in HEG focused on the external as well as internal aerodynamics including combustion of hydrogen in supersonic combustion and the investigation of transition from laminar to turbulent hypersonic flow.

1 Introduction

In hypervelocity flows the speed of the considered fluid is much larger than the speed of sound. Commonly the hypersonic flow regime is considered to start above a Mach number of M=5. Ground based testing of such flows is performed in a large variety of different types of facilities. The reason for this is the enormous range of flow conditions and phenomena encountered in hypersonic flight and the

* **Cite article as:** Deutsches Zentrum für Luft - und Raumfahrt (DLR). (2018). The High Enthalpy Shock Tunnel Göttingen of the German Aerospace Center (DLR). *Journal of large-scale research facilities, 4*, A133. http://dx.doi.org/10.17815/jlsrf-4-168

fact that no single facility can simulate all relevant flow parameters simultaneously. Therefore, in hypersonic testing, partial simulation of different flow phenomena is performed in different types of facilities.

Examples are Mach-Reynolds number simulation in cold hypersonic ground based test facilities, verification and qualification of hot structures of space vehicles in arc-heated test facilities or the investigation of the influence of chemically reacting flow past an entry or re-entry vehicle on its aerodynamic behavior in shock tunnels or shock expansion tunnels. Comprehensive overviews of ground based testing of hypersonic flows are given by e.g. Lu & Marren (2002) or Lukasiewicz (1973).

One possibility to increase the Mach number in ground based facilities is to reduce the free stream temperature, i.e. the free stream speed of sound. Here, correct similarity Mach numbers can be achieved, even though the free stream velocity is significantly lower than the actual flight velocity. However, characteristic of high Mach number hypersonic flight with $M \approx 10$ and above is that the kinetic energy of the flow is high enough to effectuate high temperature effects such as vibrational excitation or dissociation of the fluid molecules in the flow past hypersonic vehicles. The high flow velocities and subsequently the high temperature effects are not duplicated in cold hypersonic test facilities.

During the re-entry flight of a space vehicle in the earth's atmosphere or the interplanetary atmospheric entry of space vehicles or meteorites, speeds in excess of 6 km/s are achieved. To establish a flow with this speed in a test section with an area of 1 m^2 and a density of 3 g/m^3, a power requirement of already 300 MW is needed. Therefore, continuous flow facilities are not a practical way to generate such high enthalpy, hypersonic flows. Additionally, the correct simulation in ground based testing of the chemical relaxation length of the dissociation reactions of the fluid molecules occurring for example behind the strong bow shock in front of the nose of a re-entry vehicle, requires the duplication of the flight binary scaling parameter ρL; the product of the free stream density ρ times a characteristic flow length L. Consequently, the smaller the scale of the wind tunnel model is chosen, the higher the free stream density or pressure needs to be. Considering the flight trajectory range of a re-entry vehicle in about 70 km altitude, where typically the highest heat flux into the structure occurs, the atmospheric density is approximately 0.1 g/m^3. Using a geometrical scaling factor of 30, a free stream density in the ground based facility of 3 g/m^3 is required.

If a flow with the above free stream density and a velocity of 6 km/s is generated by expansion in a convergent - divergent hypersonic nozzle from a reservoir at rest without adding energy, a total specific enthalpy of about 23 MJ/kg and a nozzle reservoir pressure in the order of 90 MPa is required.
This results in a nozzle reservoir temperature of about 10000 K. It is clear that such conditions can only be achieved in impulse facilities with short flow duration.

The most successful types of facility which are able to generate high enthalpy and high pressure hypersonic flows are shock tunnels and shock expansion tunnels with typical test times of approximately 5 milliseconds and less. The principle of these facilities is to store the energy over a long period of time, therefore reducing the necessary power requirement and subsequently releasing the stored energy rapidly. Due to the high flow speeds, test times in the order of a few milliseconds are still sufficient for the development of a steady flow over a model. A reasonable, conservative correlation of the necessary test time to establish a steady flow is $\tau = 20\ L/u_\infty$, where L is the model length and u_∞ is the free stream velocity. For a test using the above mentioned flow condition and a 0.3 m long wind tunnel model, the required test time would be 1 ms.

The high pressure, high velocity flows which can be generated in shock tunnels and shock expansion tunnels makes these facilities not only suitable for the investigation of space vehicle aerothermodynamics but also for studying complete air breathing propulsion systems, particularly supersonic combustion ramjets (scramjets) at flight Mach numbers of $M = 8$ and above. In this framework it is important that in addition to the free stream Mach and Reynolds number, the correct static pressure and temperature are established in the combustor. Further, if hypersonic flight configurations are considered which can be tested at 1:1 scale, the flight free stream conditions can be

duplicated in these facilities generating the same pressure and heat flux loads as experienced in flight. In the subsequent sections, the operating conditions realized in HEG will be presented.

2 High Enthalpy Shock Tunnel Göttingen (HEG)

The HEG is a free piston driven shock tunnel and was developed and constructed in the framework of the European HERMES program over the period 1989 – 1991. It was commissioned for use in 1991, at that time being the largest facility of its type worldwide. Since then it was extensively used in a large number of national and international space and hypersonic flight projects. The research activities are always strongly linked to computational fluid dynamics (CFD) and comprise for instance the calibration process of the facility (Hannemann et al. (2003)), the study of generic aerodynamic configurations including the investigation of fundamental aspects of high enthalpy flows (Karl et al, (2004), Wagner et al. (2016)), complex hypersonic flight configurations (Karl et al. (2018)), integrated scramjet configurations (Martinez Schramm et al (2008)) and hypersonic boundary layer transition and transition control strategies (Wagner et al. (2013), Laurence et al. (2014), Sandham et al. (2014)).

In a free piston driven shock tunnel, the conventional driver of a shock tunnel is replaced by a free piston driver. This concept was proposed by Stalker (1967). A schematic and a (x,t) wave diagram of this facility type is shown in Figure 1. Free piston driven shock tunnels consist of an air reservoir behind the piston, a compression tube, separated from an adjoining shock tube via the primary diaphragm, and a subsequent nozzle, test section and dump tank.

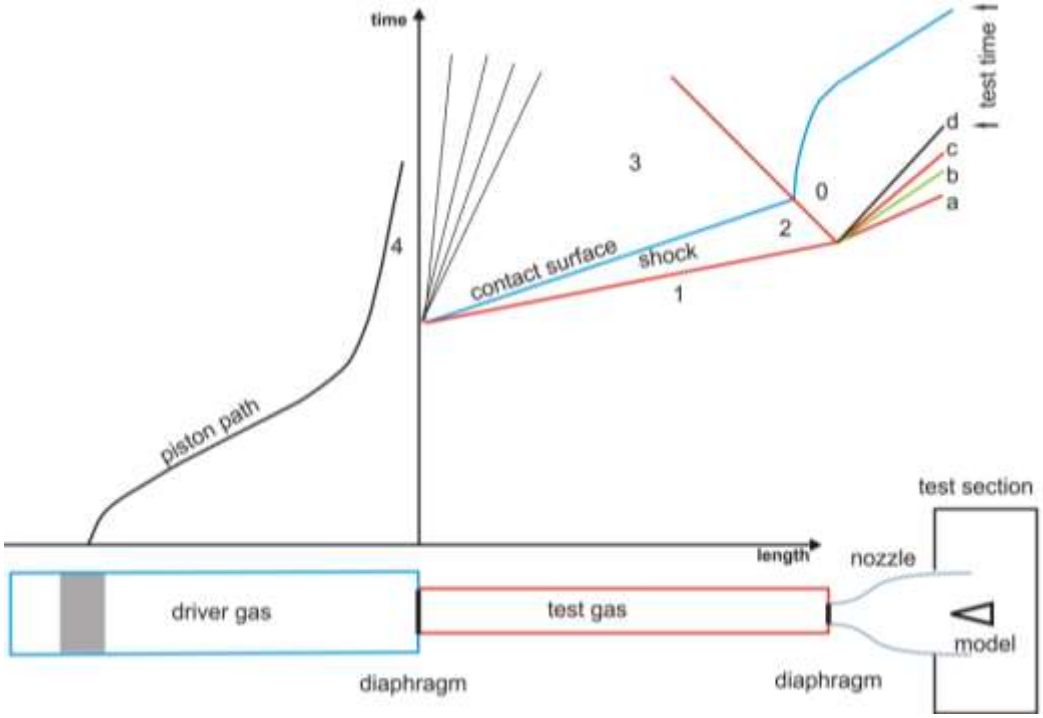

Figure 1: Schematic of a free piston driven shock tunnel and the wave (x-t) diagram.

A schematic of HEG is given in Figure 2. The high pressure air stored in the secondary reservoir is utilized to accelerate a heavy piston down the compression tube. During this quasi-adiabatic compression and heating of the light driver gas (typically Helium or a Helium Argon mixture) the piston reaches a maximum velocity in the order of 300 m/s. The driver gas temperature increases with the driver gas volumetric compression ratio. When the main diaphragm burst pressure is reached it ruptures

and the wave process as in a conventional reflected shock tunnel is initiated (see Figure 1). A shock wave is moving into the driven section and the head of a centered expansion wave is moving into the high pressure region. The numbers used in Figure 1 denote distinct regions of the flow. Region 1 contains the test gas at the initial shock tube filling conditions and region 4 contains the hot, compressed driver gas after piston compression. Region 2 contains the shock compressed test gas, while in region 3, the driver gas processed by the unsteady expansion wave is contained. The test and driver gas are separated by a contact surface.

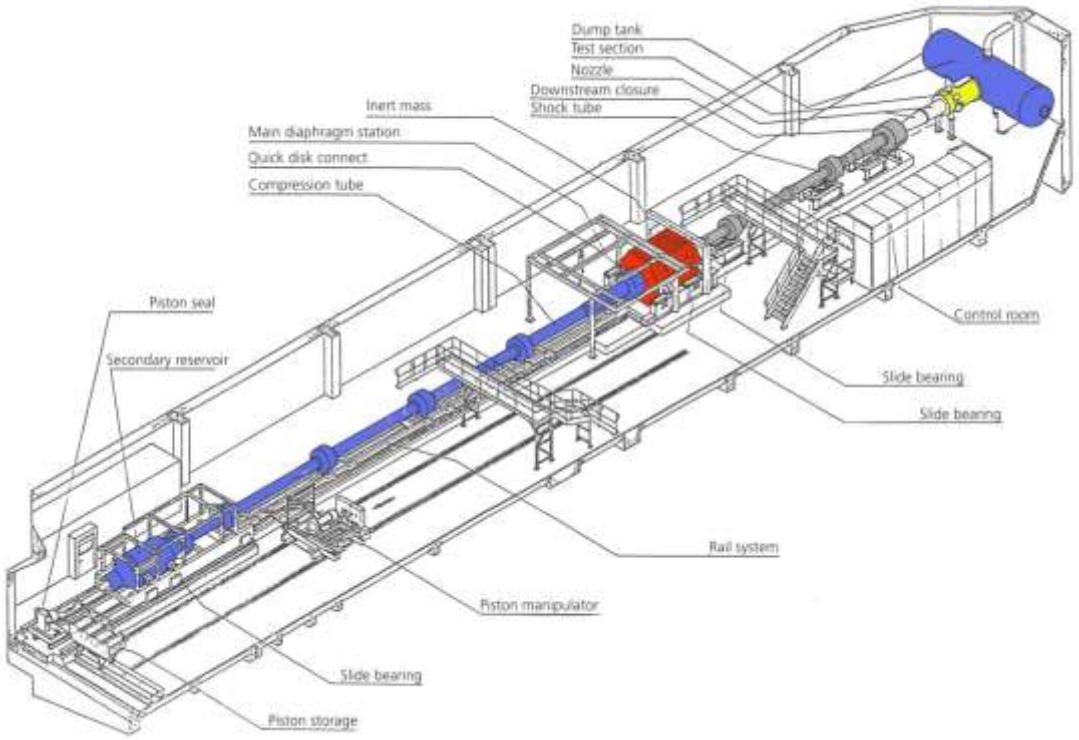

Figure 2: Schematic of the High Enthalpy Shock Tunnel Göttingen, HEG.

After reflection of the incident shock wave at the right end wall of the shock tube, the test gas is brought to rest in region 0. Subsequently, the reflected shock wave penetrates the contact surface. Depending on the local conditions, three types of shock wave / contact surface interaction can be differentiated. Due to the fact that the shock-compressed and heated slug of gas in region 0 is used in reflected shock tunnel operation as the reservoir driving the flow in the nozzle and test section, shock tube operation in tailored interface mode is most desirable. At this condition the pressure in region 0 remains constant. For undertailored or overtailored interface conditions, the pressure in region 0 is decreasing or increasing, respectively after interaction of the reflected shock with the contact surface.

Reflected shock tunnels are characterized by a convergent - divergent nozzle which is attached to the end of the shock tube. A thin secondary diaphragm is placed at the nozzle entrance in order to allow evacuation of the nozzle, test section and vacuum tank before the run. The nozzle entrance diameter is chosen sufficiently small such that the incident shock wave is almost completely reflected. The stagnant slug of test gas, generated by the shock reflection in region 0, is subsequently expanded through the hypersonic nozzle.

Figure 3: Photographic views of the High Enthalpy Shock Tunnel Göttingen, HEG.

The nozzle flow starting process is characterized by a wave system which passes through the nozzle before a steady flow is established (see Figure 1). The incident shock wave (a) is followed by a contact surface (b), an upstream facing secondary shock wave (c) and the upstream head of an unsteady expansion (d). The trajectory of the piston is chosen in a way that after main diaphragm rupture, the pressure and temperature of the driver gas in region 4 is maintained approximately constant. This is achieved by selecting the velocity of the piston at diaphragm rupture, and therefore the subsequent movement of the piston such that it compensates for the loss of the driver gas flowing into the shock tube. For that reason, in contrast to the constant volume driver of conventional shock tunnels, the free piston driver is a constant pressure driver. Due to the large forces occurring during the operation of the free piston driver, the compression tube, shock tube, nozzle assembly is allowed to move freely in axial direction. An inert mass placed at the compression tube / shock tube junction can significantly reduce the recoil motion of the facility during operation. The test section and the vacuum tank remain stationary. A sliding seal is used at the nozzle / test section interface.

The overall length of HEG is 62 m and it weighs approximately 280 t. A third of its weight is contributed by an inert mass (see Figure 2 and left picture of Figure 3) which is used to reduce the tunnel recoil motion. The compression tube is closed by a hydraulic oil system (quick disk connect) at the main diaphragm station. The shock tube is connected to the nozzle of the tunnel at the downstream closure, which is also driven by oil hydraulics to close and seal the tunnel. The compression tube has a length of 33 m and a diameter of 0.55 m. The shock tube is 17 m long with a diameter of 0.15 m. The HEG was designed to provide a pulse of gas to a hypersonic convergent - divergent nozzle at stagnation pressures of up to 200 MPa and stagnation enthalpies of up to 23 MJ/kg. Regarding the test gas, no basic limitations exist. The operating conditions presented in the present article are related to the test gas air. Additionally, operating conditions using nitrogen and carbon dioxide exist.

3 HEG Operating Conditions

Originally, HEG was designed for the investigation of the influence of high temperature effects such as chemical and thermal relaxation on the aerothermodynamics of entry or re-entry space vehicles. As discussed above, in order to correctly model the chemical relaxation occurring behind the bow shock of a re-entry vehicle the flight binary scaling parameter must be reproduced in ground based testing. Further, for high enthalpy testing an additional driving parameter which must be reproduced is the flow velocity. Therefore, the operating conditions of HEG are first discussed in Figure 4 in terms of the binary scaling parameter ρL and the flow velocity u.

Here L represents the length of the considered configurations. In addition to the HEG operating conditions (represented by the dots), the most important fluid mechanical and chemical processes occurring during re-entry of a spacecraft in the Earth's atmosphere are depicted in Figure 4. Further, as a reference the flight trajectories of a lifting body re-entry from low Earth orbit (IXV), a ballistic superorbital re-entry (Apollo 11) and a hypersonic flight experiment (SHEFEX) are provided. An indication of the corresponding flight altitudes is given in the right diagram of Figure 4 showing the temperature variation of the Earth's atmosphere. The transitions between regimes of different physical and chemical properties shown in Figure 4 depend on the chosen reference length and vary when different configurations are considered. Further, the boundaries shown have only symbolic character. In reality, no clear-cut dividing lines between the different regimes exist. The Knudsen number given in Figure 4 shows that the HEG operating conditions are located in the continuum flow regime. The high energy content of re-entry flows leads to strong heating of the air in the vicinity of a spacecraft. Depending on the temperature level behind the shock wave (i.e. the flight velocity), the vibrational degrees of freedom of the air molecules are excited and dissociation reactions of oxygen- and nitrogen molecules may occur. Further, ionization of the air constituents occurs. The high temperature effects described here are enabled by energy transfer from the translational energy stored in the random motion of the air particles, which is increased by the gas heating, to other forms of energy. Because this energy transfer is realized by air particle collisions, it requires a certain time period to develop. The time required to reach an equilibrium condition, is e.g. defined by the local temperature and density. Therefore, depending on the ratio of the relaxation time to a characteristic timescale of the flow, the chemical and thermal relaxation processes can be either in non-equilibrium or in equilibrium.

Further, along a re-entry trajectory, the Reynolds number varies over several orders of magnitude. In high altitude flight the wall boundary layer of a re-entry vehicle is initially laminar. After exceeding a critical Reynolds number (shown exemplarily for the IXV configuration in Figure 4), the transition from a laminar to a turbulent boundary layer takes place. This process is linked to an increase of the skin friction and the wall heat flux. The HEG operating conditions (depicted with nozzle 5 in Figure 4) are the original high enthalpy conditions covering a total specific enthalpy range from 12 – 23 MJ/kg. These conditions have been used for the investigation of several re-entry configurations including ARD, X-38, EXPERT, ExoMars or Pre-X / IXV.

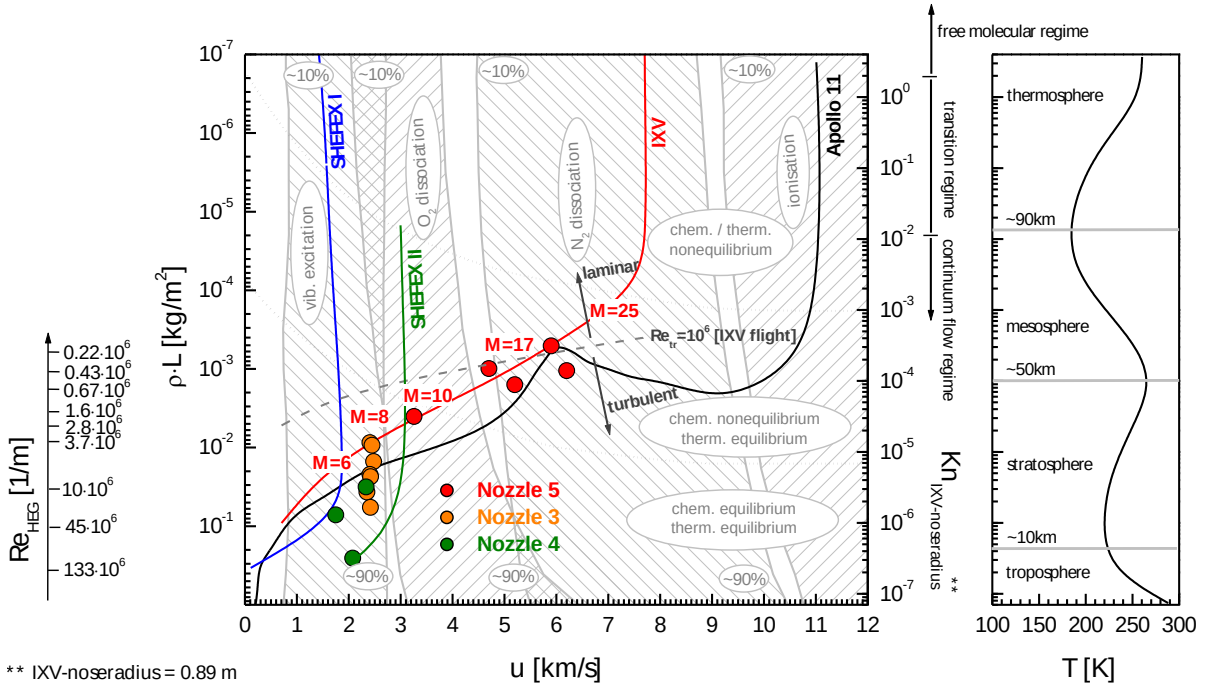

Figure 4: HEG operating range in terms of the binary scaling parameter ρL and the flow velocity u.

Over the last years the HEG operating range was subsequently extended. In this framework the main emphasis was to generate test conditions which allow investigating the flow past hypersonic flight configuration from low altitude Mach 6 up to Mach 10 in approximately 33 km altitude. These low enthalpy conditions cover the range of total specific enthalpies from 1.5 – 6 MJ/kg. For 1:1 scale wind tunnel models, conditions (with nozzle 3 depicted in Figure 4) duplicate M = 7.4 flight conditions in 28 km and 33 km, respectively. They were used for the ground based testing of the HyShot II and IV supersonic combustion flight experiment configurations as described in Martinez Schramm et al. (2008) and Karl et al. (2008).

Additional conditions (depicted with nozzle 4 Figure 4) duplicate M = 6 flight conditions between 15 km flight altitude and at sea level, respectively. These conditions were used in the framework of the SHEFEX I post flight analysis and the investigation of the intake of the LAPCAT (EC project Long-Term Advanced Propulsion Concepts and Technologies) M = 8 aircraft, Martinez Schramm et al. (2009). M = 10 condition (depicted with nozzle 5 Figure 4) duplicate flight conditions in 33 km altitude, and have been used in the framework of the DLR SHEFEX II project and for the ground based testing of a scramjet flight experiment configuration, Böhrk et al. (2012).

In Figure 5, the low enthalpy HEG operating conditions are given in terms of Mach and Reynolds number. The Reynolds number is based on the length of the considered configurations. As reference, the trajectories of the flight configurations SHEFEX I and II, HyShot II and IXV are given.

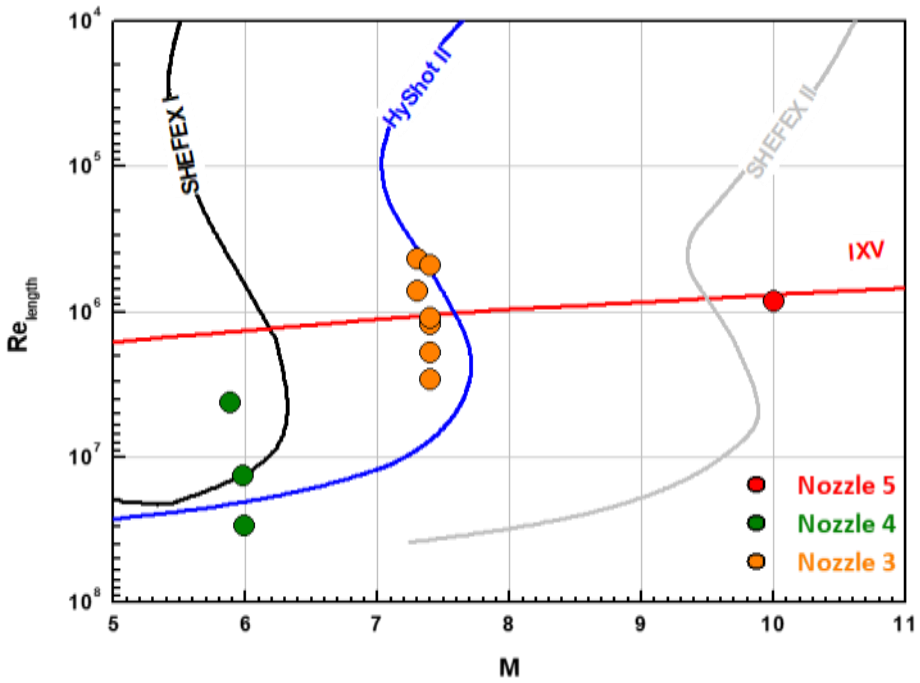

Figure 5: HEG operating conditions in terms of Mach and Reynolds number.

Details of the HEG operating conditions discussed above are provided inTable 1, Table 2 and Table 3. In order to realize the operating conditions, a series of different Laval nozzles had to be designed, constructed and implemented in HEG. The nozzle which is used to expand the test gas to the targeted free stream is given in the header of each table. The test time for the high enthalpy conditions is in the range of 1 ms. For the low enthalpy conditions, the test time ranges from 3 to 8 ms. The nozzles used to generate the corresponding test conditions are given in Figure 6. Details of the four operational HEG nozzles are provided in the following section. Further different pistons are utilized on HEG for generating different operating conditions. In order to allow a large flexibility in tuning new operating conditions, four pistons (without brakes) with different weight (275 kg, 481 kg, 700 kg and 815 kg) are available. Further one 848 kg piston with brakes is utilized.

Nozzle	2				5
Condition	H22R0.20	H23R0.42	H12R0.39	H15R0.67	H6R2.8
p_0 [MPa]	35	85	44	90	70
T_0 [K]	9100	9900	7000	8100	4400
h_0 [MJ/kg]	22	23	12	15	6
M_∞ [-]	8.2	7,8	8.1	7.9	10.3
Re_m [1/m· 10^6]	0.2	0.42	0,39	0.67	2.8
p_∞ [Pa]	660	1700	790	1680	930
T_∞ [K]	1140	1450	800	1060	253
ρ_∞ [g/m^3]	1.7	3.5	3.3	5.3	12.6
u_∞ [m/s]	5900	6200	4700	5200	3270

Table 1: Operating conditions using nozzle 2 and 5. The former condition nomenclature is from left to right I, II, III, IV and XXXI.

Nozzle	3								
Condition	H3.3R1.5	H3.4R1.6	H3.5R2.4	H3.3R3.7	H3.2R4.1	H3.0R6.4	H3.4R9.8	H11.9R1.5	H9.8R2.2
p_0 [MPa]	6.8	8.0	12.7	17.0	19.2	28.4	47.3	37.6	44.1
T_0 [K]	2720	2810	2895	2740	2734	2582	2835	6816	5932
h_0 [MJ/kg]	3.3	3.4	3.5	3.3	3.2	3.0	3.4	11.9	9.8
M_∞ [-]	7.3	7.4	7.3	7.4	7.4	7.4	7.4	6.1	6.2
Alt (p_∞) [km]	32.8	32.0	28.7	26.6	26.1	23.8	20.4	18.7	18.0
Re_m [1/m· 10^6]	1.5	1.6	2.4	3.7	4.1	6.4	9.8	1.5	2.2
p_∞ [Pa]	789	880	1453	1990	2129	3083	5174	6761	7460
T_∞ [K]	267	277	285	266	268	248	265	1333	1084
ρ_∞ [g/m^3]	10.2	11.0	17.7	25.9	27.6	43.2	67.8	16.9	23.5
u_∞ [m/s]	2409	2450	2480	2410	2422	2350	2419	4426	4036

Table 2: Operating conditions using nozzle 3. Former condition nomenclature is XIV for H3.4R1.6, XIII for H3.3R3.7, XV for H3.0R6.4 and XVII for H3.5R2.4.

Nozzle	4				
Condition	H3.2R14	H2.0R35	H1.5R45	H2.5R101	H2.6R133
p_0 [MPa]	30	32	37	161	188
T_0 [K]	2690	1800	1640	2120	2220
h_0 [MJ/kg]	3.2	2	1.5	2.5	2.6
M_∞ [-]	5.7	6	6	5.8	6
Alt (p_∞) [km]	12.7	12.2	11.8	1.4	0.3
Re_m [1/m· 10^6]	14	35	45	101	133
p_∞ [Pa]	17540	18815	20100	86249	97800
T_∞ [K]	422	208	221	306	292
□$_\infty$ [g/m^3]	144	315	327	977	1160
u_∞ [m/s]	2336	1744	1750	2066	2077

Table 3: Operating conditions using nozzle 4. Former condition nomenclature is XXI for H1.5R45 and XXII for H2.6R133.

4 Set of HEG Nozzles

The set of HEG nozzles comprises of a conical nozzle used for the high enthalpy conditions I-IV and three contoured nozzles for the low enthalpy conditions. Their nominal design Mach number, area ratio and length are given in Figure 6. Please note that for nozzle 2 the Mach number is lower than the corresponding flight Mach number due to chemical and thermal freezing effects during the nozzle expansion.

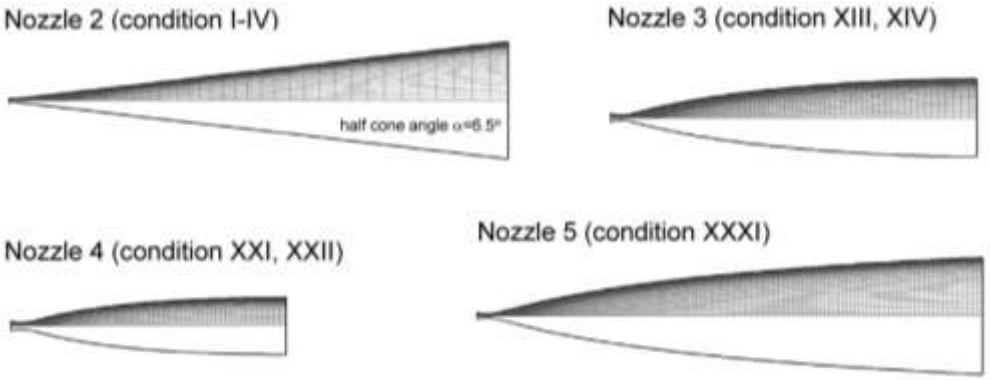

Nozzle	2	3	4	5
nominal M	8	8	6	10
d*[mm]	22	40	50	26
$d_{E,ist}$[mm]	880	590	430	880
$A_{E,ist}/A^*$	1600	218	74	1146
L [mm]	3780	2710	2015	3780

Figure 6: Geometries of the HEG nozzles.

However, for high enthalpy testing the Mach number is of less importance and the flight velocity must be reproduced correctly.

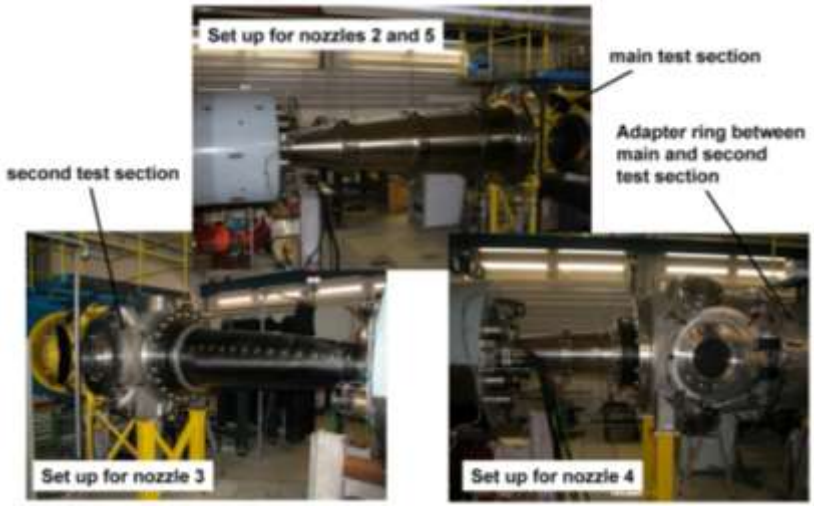

Figure 7: HEG nozzle – test section assembly.

Due to the different nozzle length, a second test section was built for nozzle 3. When utilizing nozzle 4, an additional adapter ring is used between the second and the main test section. The length and diameter of the original test section is 1.6 m and 1.2 m, respectively. The second test section is a copy of the original test section with slightly reduced dimensions (1.0 m length and 1.0 m diameter). The adapter

ring has a length of 0.8 m and a diameter 1.0 m. The nozzle – test section assembly using the four HEG nozzles is shown in Figure 7. Depending on the used operating condition and the angle of attack, model configurations with a typical length between 0.4 m and 1.0 m and a width of up to 0.4 m can be mounted in the test sections. In case the major emphasis of the tunnel testing is on the investigation of internal flow paths (e.g. scramjet combustors), models of up to 2.0 m length can be used. The weight of the models is typically less than 200 kg.

5 HEG Infrastructure

The data acquisition system of HEG consists of a total of 200 channels, data can be sampled with up to 50 MHz per channel with 16 Bit resolution (SATURN System, AMOtronics GmbH). A gaseous hydrogen injection system was installed at HEG in order to allow the delivery of hydrogen fuel to wind tunnel models for the investigation of scramjet combustion. The fuel system consists of a 12 mm diameter and 38.4 m long Ludwieg tube, and a fast acting solenoid valve. The maximum filling pressure of the Ludwieg tube is 15 MPa and it can deliver a pulse of fuel with constant pressure for up to 50 ms. A new modular cross arm calibration rake was designed and manufactured which can be used for the detailed calibration of the test section free stream flows generated by nozzles 2 – 5. Pitot pressure, static pressure and stagnation point heat transfer gauges can be mounted on this rake (see Figure 8).

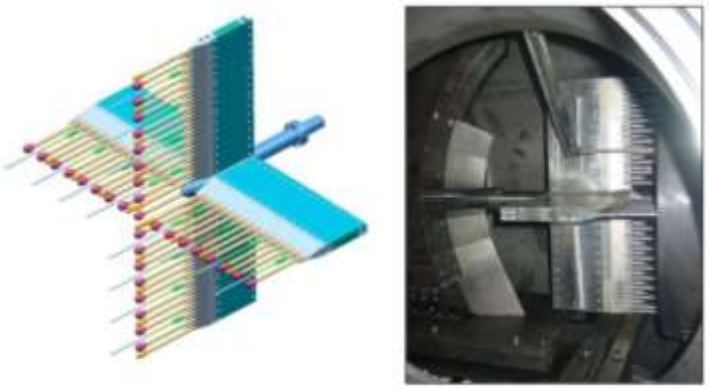

Figure 8: HEG calibration rake – design drawing (left) and rake installed in the test section (right).

6 Calibration Procedure of HEG Operating Conditions

The calibration process of new operating conditions requires a close cooperation between calibration measurements and CFD. This process is discussed here exemplarily for the HEG condition H3.3R3.7. The numerical determination of the HEG free stream consists of two steps which require a suitable set of input parameters. First, the nozzle reservoir temperature is computed with a one-dimensional analysis of the shock tube. The relevant input parameters are the measured values of the initial shock tube filling pressure and temperature, the shock speed and the nozzle reservoir pressure. Based on these nozzle reservoir conditions, the free stream is subsequently determined by numerical simulation of the nozzle flow using the DLR TAU code. Different RANS turbulence models were applied along with thermal equilibrium and non-equilibrium computations to determine the influence of different modelling assumptions on the computed free stream conditions. It should be noted that for condition H3.3R3.7, the chemical relaxation process is in equilibrium and no free stream dissociation exists. The computational grid consisting of about 20,000 grid points and the Mach number contours resulting from the thermal non-equilibrium computation are shown in Figure 9.

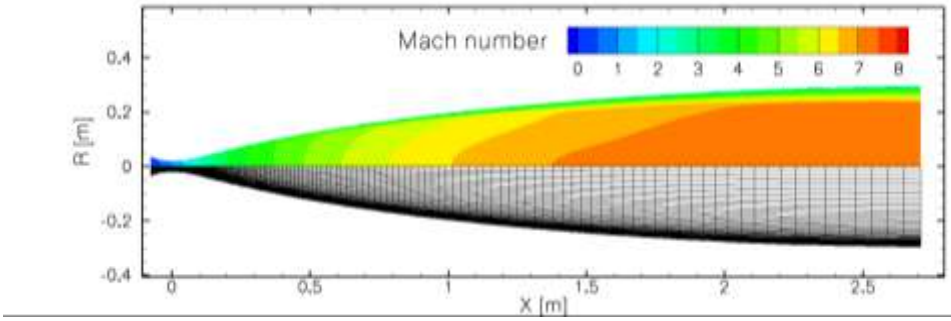

Figure 9: CFD grid and Mach number contours for the HEG nozzle flow (Condition H3.3R3.7).

A reservoir-pressure inflow boundary condition is used at the subsonic inflow of the nozzle. The thermodynamic conditions at the inflow are computed using isentropic expansion from prescribed nozzle stagnation conditions using the inflow velocity vector which is part of the CFD solution. The nozzle supply conditions for the considered HEG operating condition H3.3R3.7 is given in Table 2. The chemical non-equilibrium 5 species and 17 reactions rate set for air proposed by Gupta was applied, see Karl et al. (2008). The considered species are molecular and atomic nitrogen and oxygen (N2, O2, N, O) and nitric oxide (NO). The CFD results are subsequently compared with Pitot pressure and stagnation heat flux measurements on spherical probes and static pressure measurements obtained with the HEG calibration rake.

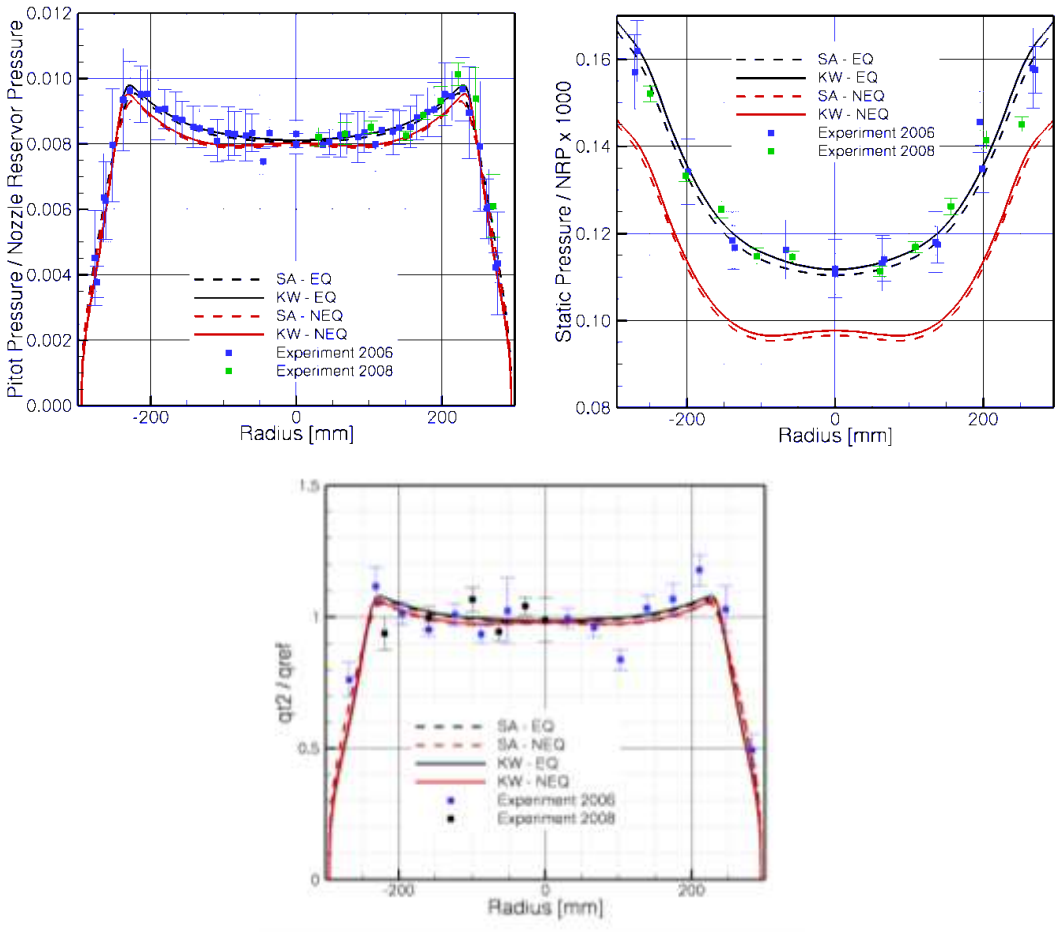

Figure 10: Comparison of measured and computed normalized Pitot pressure (left), static pressure (middle) and stagnation point heat flux distributions at the nozzle exit plane; NEQ: thermal non-equilibrium, EQ: thermal equilibrium, SA: Spalart-Allmaras turbulence model, KW: Wilcox k-ω turbulence model, NRP: Nozzle reservoir pressure (HEG operating condition H3.3R3.7).

In Figure 10, the comparison of the measured and computed Pitot pressure, static pressure and stagnation point heat transfer profiles at the nozzle exit plane are shown for HEG condition H3.3R3.7. Regarding the Pitot pressure, the computed data resulting from calculations assuming a thermal equilibrium or thermal non-equilibrium nozzle expansion lie within the experimental scatter bars. The wall boundary layer is assumed to be fully turbulent and the difference due to the application of different turbulence models is negligible. The best agreement between computed and measured Pitot pressure profiles is obtained with the thermal equilibrium assumption and the Wilcox k-ω turbulence model. The computed static pressure profiles reveal pronounced deviations resulting from the application of different thermal relaxation models. Based on these results it was concluded that the nozzle expansion is in thermal equilibrium. Again, excellent agreement of the numerical and experimental results was achieved using the Wilcox k-ω turbulence model and the thermal equilibrium assumption. This result shows the importance of performing static pressure measurements even at total specific enthalpy conditions of approximately 3 MJ/kg. The bottom plot of Figure 10 shows the comparison of the numerical and experimental normalized stagnation point heat flux profiles. Good agreement with the rake measurements are obtained, however, similar to the Pitot pressure, the stagnation point heat flux measurements are not sensitive to the modelling of the thermal relaxation in the nozzle flow.

7 Measurement Techniques Overview

The well-established measurement techniques at HEG comprising of surface pressure and heat flux measurements, phase step holographic interferometry and the high speed flow visualisation system (Schlieren / Shadowgraph) are described e.g. in Tropea (2007). A recently proposed probe to measure free-stream disturbances in shock tunnels is introduced in Wagner et al. (2018).

The high speed flow visualization system can be used in conjunction with a digital high speed camera for instance a Shimadzu HPV-1, a Phantom V1210, a Phantom V2012 or a Photron FASTCAM SA-Z type 2100K. The Shimadzu HPV-1 camera is able to record up to 100 frames at a maximum imaging rate of 1 MHz with a resolution of 312x260, while the Phantom V2012 offers a resolution of maximal 1280x800 pixels with an imaging rate of 22.5 kHz. The Photron FASTCAM SA-Z allows a resolution of 1024x1024 pixels at a sampling rate of 20 kHz. The resolution of the latter two cameras can be reduced to achieve significantly higher imaging rates of up to 2.1 MHz. The shuttering of the images is usually achieved by the pulsed laser sources and can be adjusted down to 10 ns for high frequencies (Cavitar Cavilux HF systems).

An internal multiple component stress wave force balance was designed, calibrated and tested in HEG. The balance is able to measure forces (approximately 50 to 5000 N) within 1 - 5 ms on instrumented models at angles of attack from -40° to 20°. The accuracy of the force balance is estimated at approximately ±5% for the axial component and ±4% for the normal and pitching moment components (Robinson et al. (2006)). Additional force measurement techniques based on external stress wave force balances, accelerometer based and free flight based force measurement techniques have been developed and implemented in the past years. A description of the development evolution is given by Friedl et al. (2015) and Laurence et al. (2018).

The development of the application of temperature sensitive paints (TSP) to determine wall heat flux in HEG resulted in an applicable system which can be used for low enthalpies so far an is described in Ozawa et al. (2015).

Recently, particle image velocimetry (PIV) was applied in HEG at a total specific enthalpy of 3.3 MJ/kg. The measured free stream velocity of 2275 m/s agreed to within 2.3% with the computed value, see Kirmse et al. (2009).

References

Boehrk, H., Wartemann, V., Martinez Schramm, J., Wagner, A., Hannemann, K. and Eggers, T. (2012). Shock Tunnel Testing of the Transpiration-Cooled Heat Shield Experiment AKTiV. In *18th AIAA International Space Planes and Hypersonic Systems and Technologies Conference, AIAA/3AF*. https://doi.org/10.2514/6.2012-5935

Friedl, D., Martinez Schramm, J., Hannemann, K. (2016, Juni). Measurement of Aerodynamic Coefficients of Blunt Cones at the High Enthalpy Shock Tunnel Göttingen. In *11th International Workshop on Shock Tube Technology*.

Hannemann, K. (2003). High Enthalpy Flows in the HEG Shock Tunnel: Experiment and Numerical Rebuilding. In *41st AIAA Aerospace Sciences Meeting and Exhibit, AIAA 2003-0978*. https://doi.org/10.2514/6.2003-978

Karl, S., Martinez Schramm, J. and Hannemann, K. (2004). Experimental and Numerical Investigation of High Enthalpy Flow Past a Cylinder in HEG. In *24th International Symposium on Shock Waves*. Berlin, Heidelberg: Springer. https://doi.org/10.1007/978-3-540-27009-6_24

Karl, S., Hannemann, K., Mack, A., Steelant. J. (2008). CFD Analysis of the HyShot II Scramjet Experiments in the HEG Shock Tunnel. In *15th AIAA International Space Planes and Hypersonic Systems and Technologies Conference, AIAA 2008-2548*. https://doi.org/10.2514/6.2008-2548

Karl, S., Steelant, J. (2018). Crossflow Phenomena in Streamline-Traced Hypersonic Intakes. *Journal of Propulsion and Power, 34*(2), 449-459. https://doi.org/10.2514/1.B36637

Kirmse, T., Schröder, A., Martinez Schramm, J., Karl, S. and Hannemann, K. (2009). Application of Particle Image Velocimetry and the Background Oriented Schlieren Technique in the High Enthalpy Shock Tunnel Göttingen HEG. In *27th International Symposium on Shock Waves*. Berlin, Heidelberg: Springer. https://doi.org/10.1007/s00193-011-0314-2

Laurence, S., Wagner, A. and Hannemann, K. (2014). Schlieren-based techniques for investigating instability development and transition in a hypersonic boundary layer. *Experiments in Fluids, 55*(8). https://doi.org/10.1007/s00348-014-1782-9

Laurence, S., Butler, C.S., Martinez Schramm, J. and Hannemann, K. (2018). Force and Moment Measurements on a Free-Flying Capsule in a Shock Tunnel. *Journal of Spacecraft and Rockets, 55*(2), 403-414. https://doi.org/10.2514/6.2018-5385

Lu, F.K., Marren, D.E. (Eds.). (2002). *Advanced Hypersonic Test Facilities. Progress in Astronautics and Aeronautics, Volume 198*. Reston: AIAA.

Lukasiewicz, J. (1973). *Experimental Methods of Hypersonics*. New York: Marcel Dekker, Inc. https://doi.org/10.1017/S0001924000041919

Martinez Schramm, J., Karl, S., Hannemann, K. and Steelant, J. (2008). Ground testing of the HyShot II Scramjet Configuration in HEG. In *15th AIAA Int. Space Planes and Hypersonic Systems and Technology Conference, AIAA 2008-2547*. https://doi.org/10.2514/6.2008-2547

Martinez Schramm, J., Wagner, A., Wolfram, J., Hannemann, K., Barth, T., Mulot, J.-D. and Schröder, A. (2009). Post flight analysis of SHEFEX I: Shock tunnel testing and related CFD analysis. In *16th AIAA/DLR/DGLR International Space Planes and Hypersonic Systems and Technologies Conference*. https://doi.org/10.2514/6.2009-7216

Ozawa, H., Laurence, S., Martinez Schramm, J., Wagner, A. and Hannemann, K. (2015). Fast response temperature sensitive paint measurements on a hypersonic transition cone. *Experiments in Fluids, 56*(1), 1853. https://doi.org/10.1007/s00348-014-1853-y

Robinson, M., Hannemann, K. (2006). Short Duration Force Measurements in Impulse Facilities. In *25th AIAA Aerodynamic Measurement Technology and Ground Testing Conference, AIAA 2006-3439*. https://doi.org/10.2514/6.2006-3439

Sandham, N. D., Schülein, E., Wagner, A., Willems, S. and Steelant, J. (2014). Transitional shock-wave/boundary-layer interactions in hypersonic flow. *Journal of Fluid Mechanics, 752*, 349-382. https://doi.org/10.1017/jfm.2014.333

Stalker, R.J. (1967). A Study of the Free-Piston Shock Tunnel. *AIAA Journal, 5*(12), 2160-2165. https://doi.org/10.2514/3.4402

Tropea, C., Yarin, A.L., Foss, J.F. (Eds.). (2007). *Springer Handbook of Experimental Fluid Mechanics*, Berlin, Heidelberg: Springer.

Wagner, A., Kuhn, M., Martinez Schramm, J. and Hannemann, K. (2013). Experiments on passive hypersonic boundary layer control using ultrasonically absorptive carbon-carbon material with random microstructure. *Experiments in Fluids, 54*(10), 1606. https://doi.org/10.1007/s00348-013-1606-3

Wagner, A., Schramm Martinez, J., Hickey, J.P. and Hannemann, K. (2016). Hypersonic Shock Wave Boundary Layer Interaction Studies on a Flat Plate at Elevated Surface Temperature. In *22nd International Shock Interaction Symposium*. Retrieved from: http://www.gla.ac.uk/conferences/shockinteractionsymposium/

Wagner, A., Schülein, E., Petervari, R., Hannemann, K., Ali, Syed R. C., Cerminara, A. and Sandham, N. D. (2018). Combined free-stream disturbance measurements and receptivity studies in hypersonic wind tunnels by means of a slender wedge probe and direct numerical simulation. *Journal of Fluid Mechanics, 842*, 495-531. https://doi.org/10.1017/jfm.2018.132